Supplement of Atmos. Chem. Phys., 24, 12943–12962, 2024
https://doi.org/10.5194/acp-24-12943-2024-supplement

Atmospheric Chemistry and Physics
Open Access

Supplement of

The atmospheric oxidizing capacity in China – Part 2: Sensitivity to emissions of primary pollutants

Jianing Dai et al.

Correspondence to: Guy P. Brasseur (guy.brasseur@mpimet.mpg.de)

Table S1. Chemical species in the emission input of MOZART/MOSAIC scheme

	Chemical species in emission input [a]
NO_x	E_NO, E_NO2
AVOCs	E_C2H4, E_C3H6, E_BIGENE, E_C2H6, E_C3H8, E_BIGALK, E_BENZENE, E_TOLUENE, E_XYLENE, E_C2H2, E_MACR, E_CH3CHO, E_C2H5OH, E_CH3OH, E_C10H16, E_CH3COCH3, E_MVK
Other	E_CO, E_NH3, E_SO2

Notes: [a]inputs of anthropogenic emissions is obtained from MEIC emission inventory.

Table S2. Speciation of OVOCs species

OVOCs	Species [a]
Ketones	MVK, ACET, ACETOL, MEK
Alcohols	CH3OH, C2H5OH'
Formaldehydes	HCHO
Oth. aldehydes	CH3CHO, MACR, HYDRALD, OPEN, BALD
Glyoxal	GLY, MGLY
Org. nitrates	ONITR, ONIT
PAN	PAN, MPAN
Org. peroxides	C3H6OOH, C2H5OOH, PROOH, ISOOH, ALKOOH, ROOH, TERP2OOH, XYLENOOH, BENZOOH, BZOOH, XYLOLOOH, XOOH, MEKOOH, TOLOOH, MBOOOH, TERPOOH, CH3OOH, MVKOOH, PHENOOH, C6H5OOH, HOCH2OO

Notes: [a] specific OVOCs species are obtained from the WRF-Chem v 4.1.2 with the gas-phase scheme MOZART.

Table S3. Percentage of grid cells in different ozone sensitivity regimes

	Ozone sensitivity regimes	*BASE*	*NOx*	*AVOCs*	*N+A*	*TOTAL*
Winter	VOC-limited	20.1%	17.0%	21.3%	18.4%	18.4%
	NO_x-limited	68.8%	71.9%	67.9%	70.3%	70.3%
	Transition	11.2%	11.1%	10.7%	11.3%	11.2%
Summer	VOC-limited	3.4%	2.9%	3.7%	3.0%	3.0%
	NO_x-limited	91.6%	92.8%	91.3%	92.5%	92.5%
	Transition	4.9%	4.3%	5.0%	4.5%	4.4%

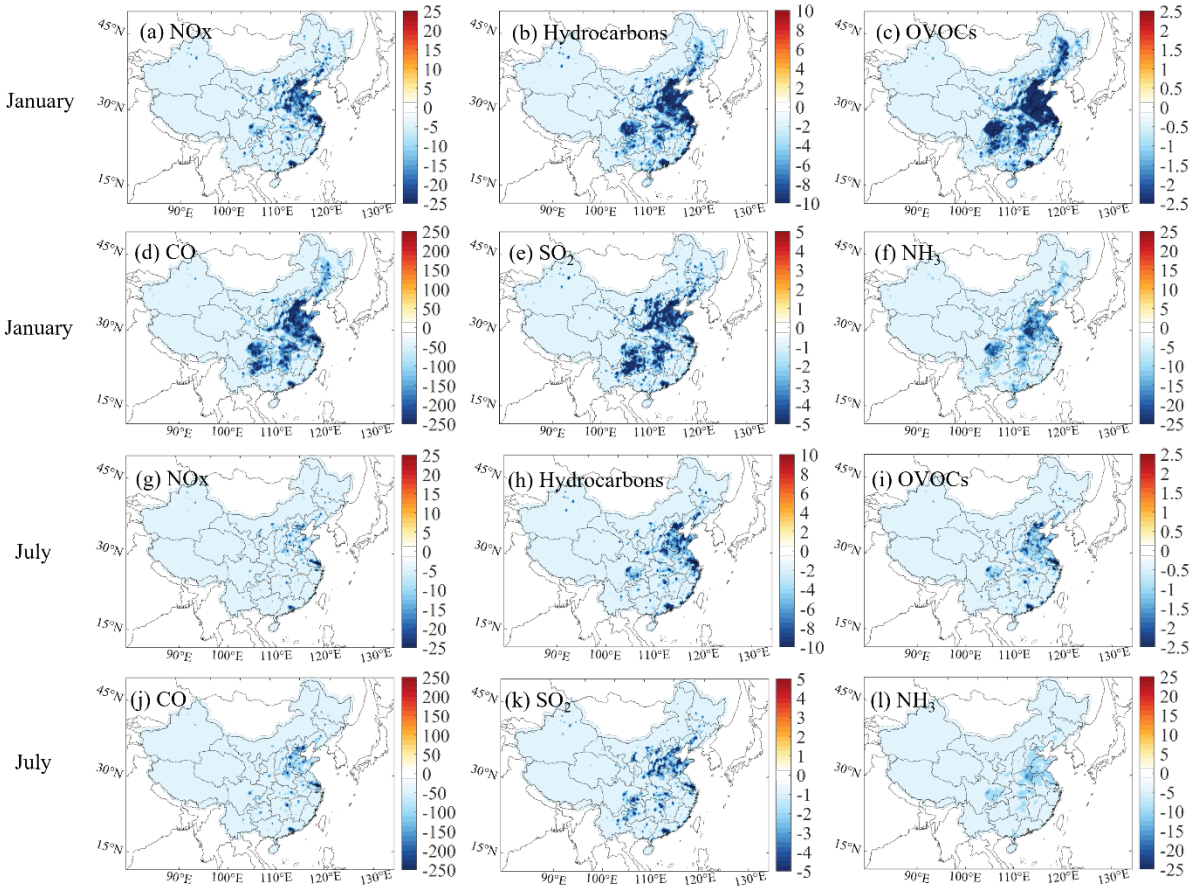

Figure S1. Changes in the monthly-averaged the model input of anthropogenic nitrogen oxides (NO_x; a, g), Hydrocarbons (b, h), oxidized volatile organic components (OVOCs; c, i), carbon monoxide (CO; d, j), sulphur dioxide (SO_2; e, k), and ammonia (NH_3; f, l) in January and July of 2018. Units are in mole km^{-2} hr^{-1}.

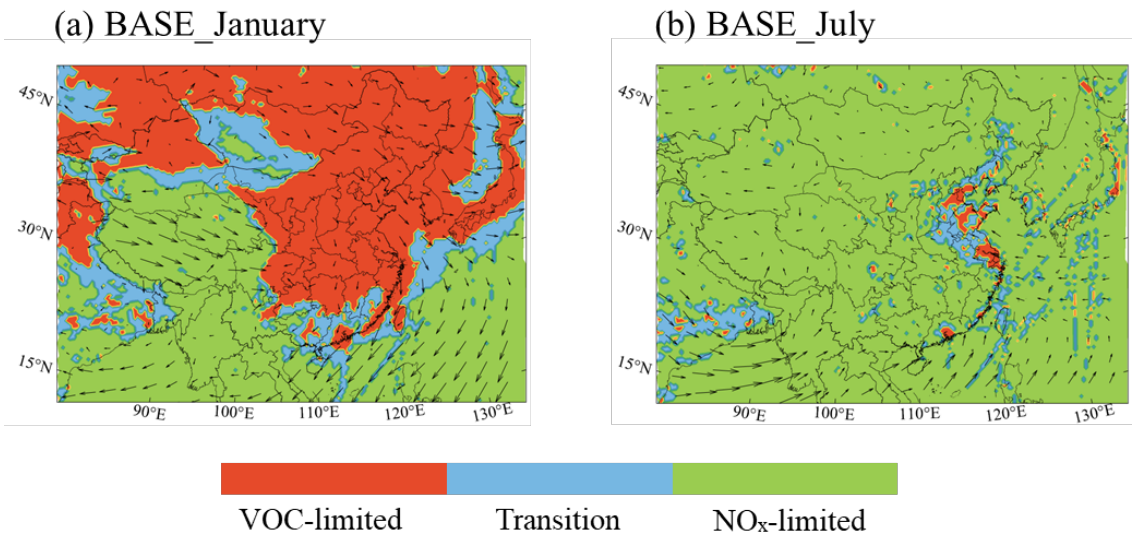

Figure S2. Display of regions in which ozone production is limited by the availability of nitrogen oxides (NO_x-limited, in green), and volatile organic components (VOC-limited, in red) under the emissions in case of BASE conditions in January (a) and July (b) of 2018.

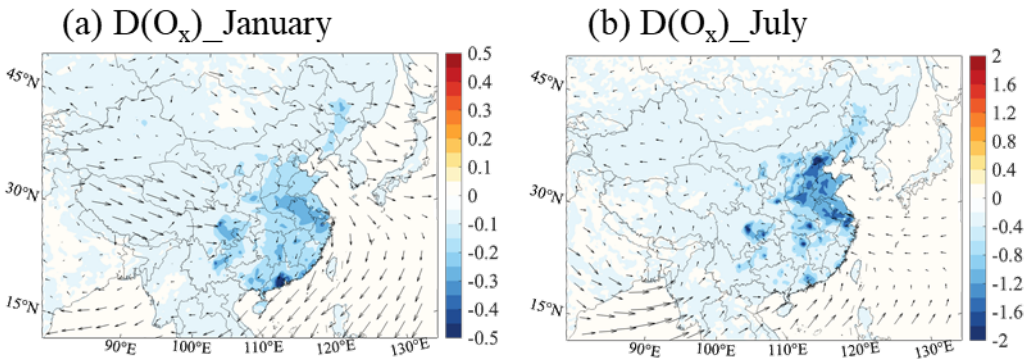

Figure S3. Changes in the monthly-averaged daytime destruction rate of odd oxygen ($D(O_x)$, Unit: ppbv h^{-1}) due to the reduction in the NO_x emissions by 50% in January (a) and July (b) of 2018.

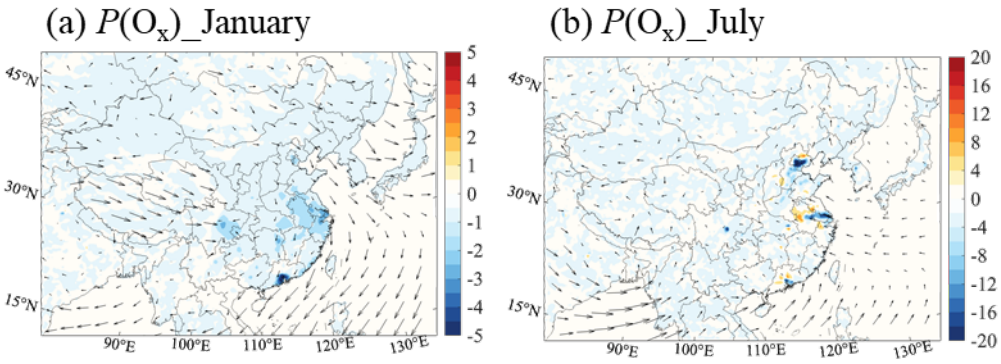

Figure S4. Changes in the monthly-averaged daytime production rate of odd oxygen ($P(O_x)$, Unit: ppbv h^{-1}) due to the reduction in the AVOCs emissions by 50% in January (a) and July (b) of 2018.

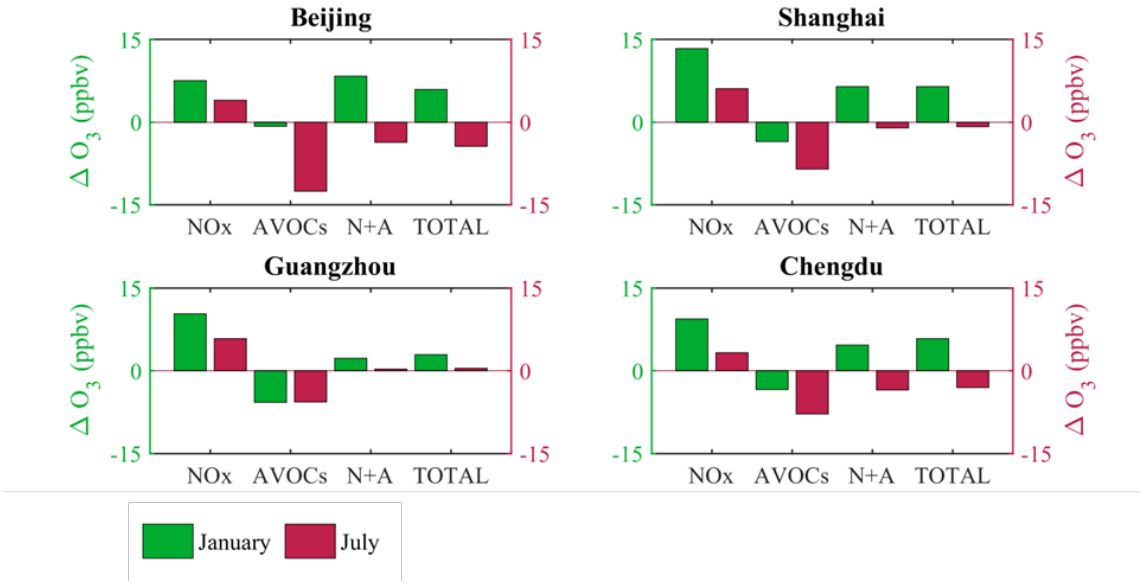

Figure S5. Changes in the monthly-averaged daytime ozone concentration (Unit: ppbv) response to the NOx, AVOCs, N+A, and TOTAL cases at four city sites in January and July of 2018.

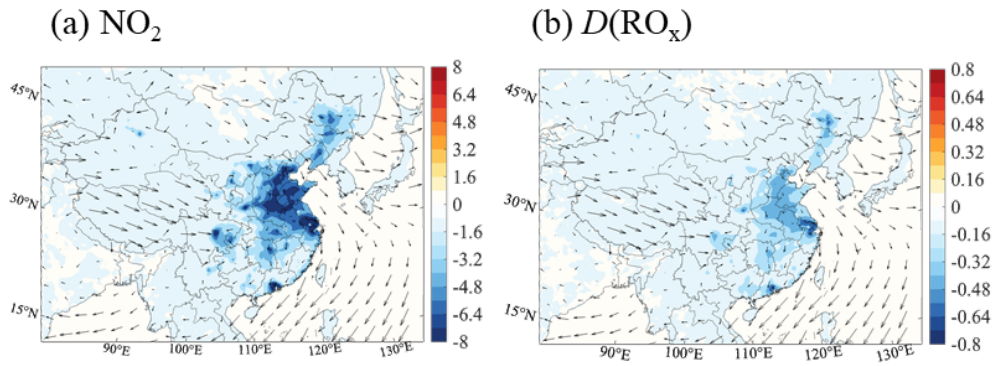

Figure S6. Changes in the monthly-averaged concentration of NO_2 (a) [Unit: ppbv] and the destruction rate of radical from the reaction of NO_2 with OH (b) [Unit: ppbv h^{-1}] surface response to the reduction in the NO_x emission by 50% (*NOx* case) relative to *BASE* case in January of 2018. Arrows represent the wind speed and wind direction.

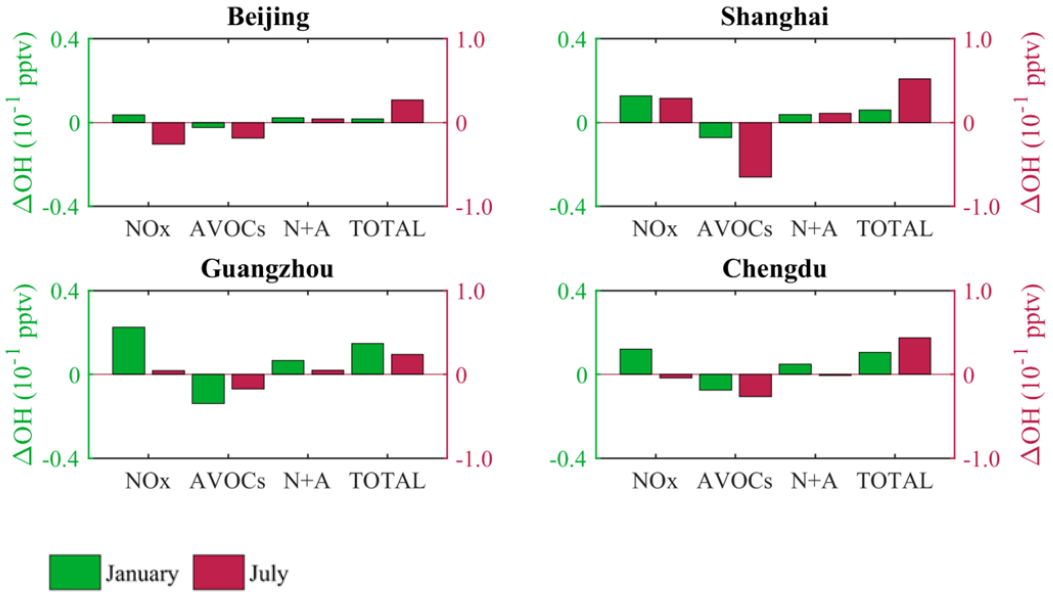

Figure S7. Changes in the monthly-averaged daytime mixing ratio of OH radical (Unit: 0.1 ppbv) response to the NOx, AVOCs, N+A, and TOTAL cases at four city sites in January and July of 2018.

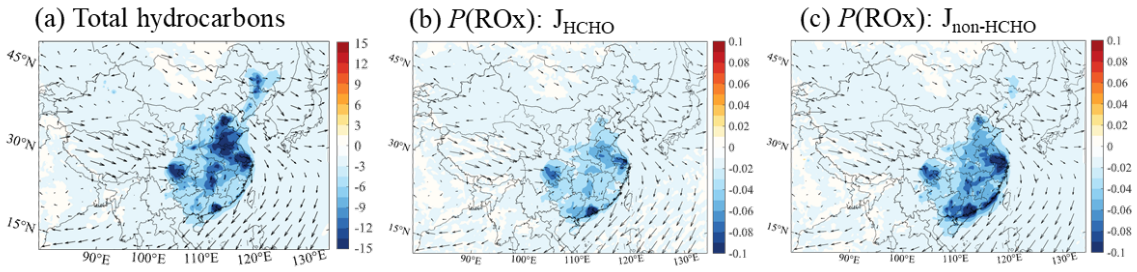

Figure S8. Changes in the monthly-averaged concentration of hydrocarbons (a) [Unit: ppbv] and the production rate of radical from the photolysis of formaldehyde (HCHO) (b) [Unit: ppbv h^{-1}] and non-HCHO OVOCs (c) [Unit: ppbv h^{-1}] response to the reduction in the AVOCs emission by 50% (*AVOCs* case) relative to *BASE* case in January of 2018. Arrows represent the wind speed and wind direction.

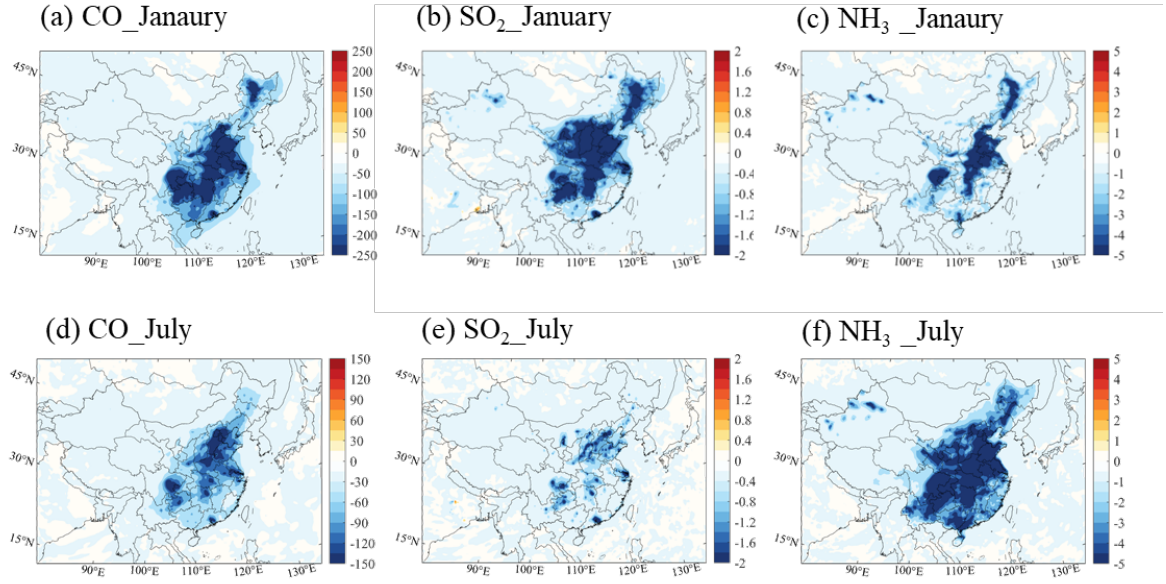

Figure S9. Changes in the monthly-averaged concentration of CO (a, d) [Unit: ppbv], SO_2 (b, e) [Unit: ppbv], and NH_3 (c, f) [Unit: ppbv] response to the TOTAL case relative to the N+A case in January (a-c) and July (d-f) of 2018.

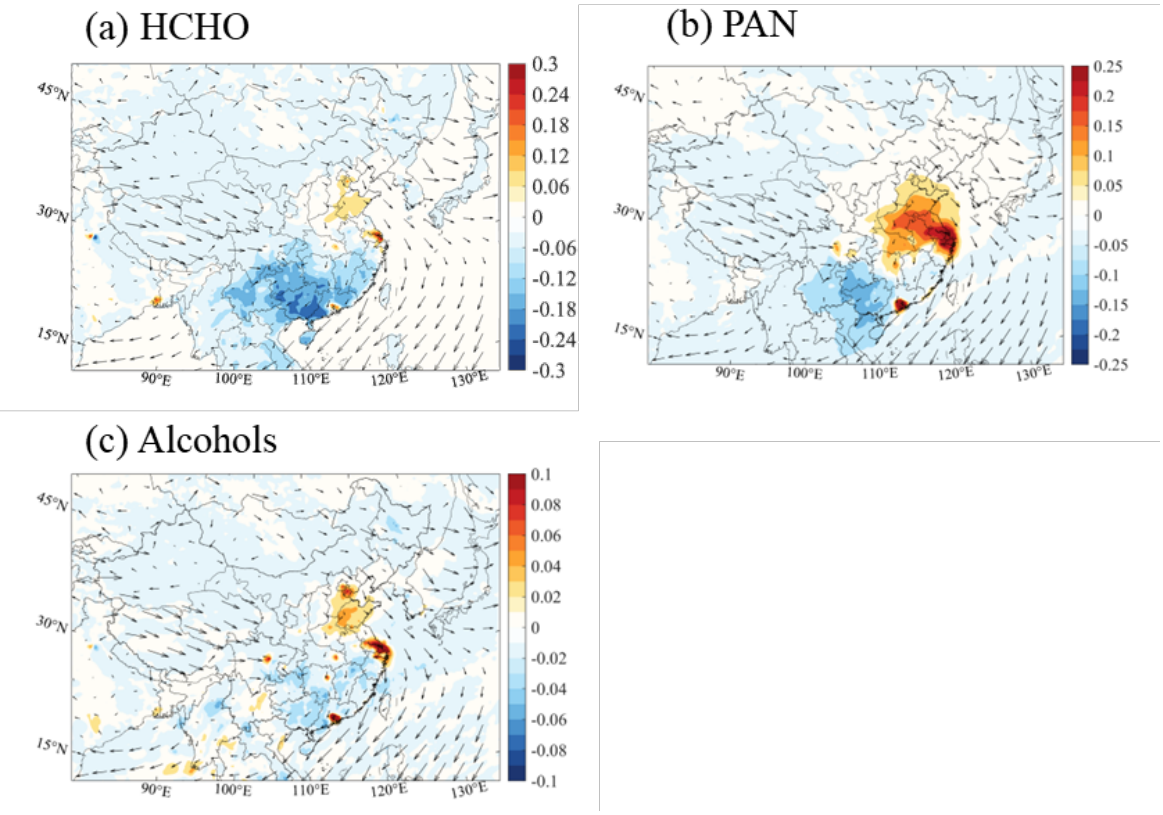

Figure S10. Changes in the monthly-averaged concentration of formaldehyde (HCHO) (a) [Unit: ppbv], peroxyacetyl nitrate (PAN) (b) [Unit: pptv], and alcohols (the sum of CH_3OH and C_2H_5OH) (c) [Unit: ppbv] response to the reduction in emission of NO_x relative to *BASE* case in January 2018. Arrows represent the wind speed and wind direction.

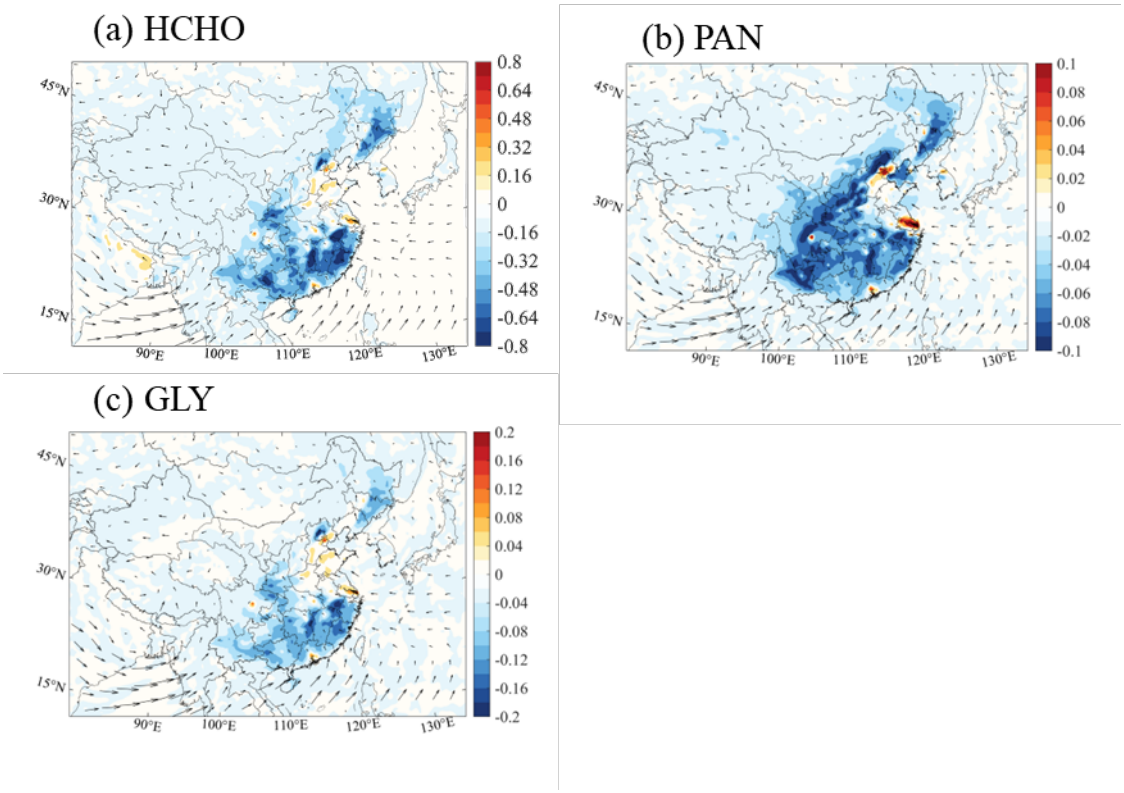

Figure S11. Changes in the monthly-averaged concentration of formaldehyde (HCHO) (a) [Unit: ppbv], peroxyacetyl nitrate (PAN) (b) [Unit: pptv], and glyoxal (GLY) (c) [Unit: ppbv] response to the reduction in emission of NO_x relative to *BASE* case in July 2018. Arrows represent the wind speed and wind direction.

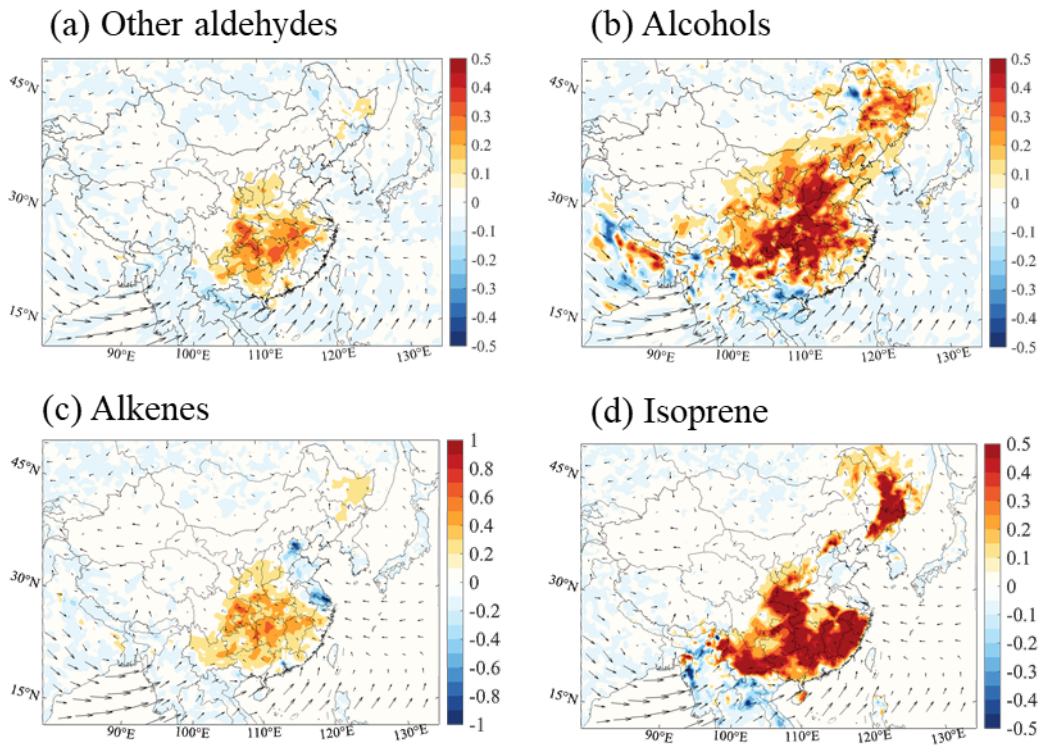

Figure S12. Changes in the monthly-averaged concentration of other aldehydes (aldehydes except for HCHO) (a) [Unit: ppbv], alcohols (b) [Unit: pptv], alkenes (c) [Unit: ppbv], and isoprene (d) [Unit: ppbv] response to the reduction in emission of NO_x relative to *BASE* case in July 2018. Arrows represent the wind speed and wind direction.

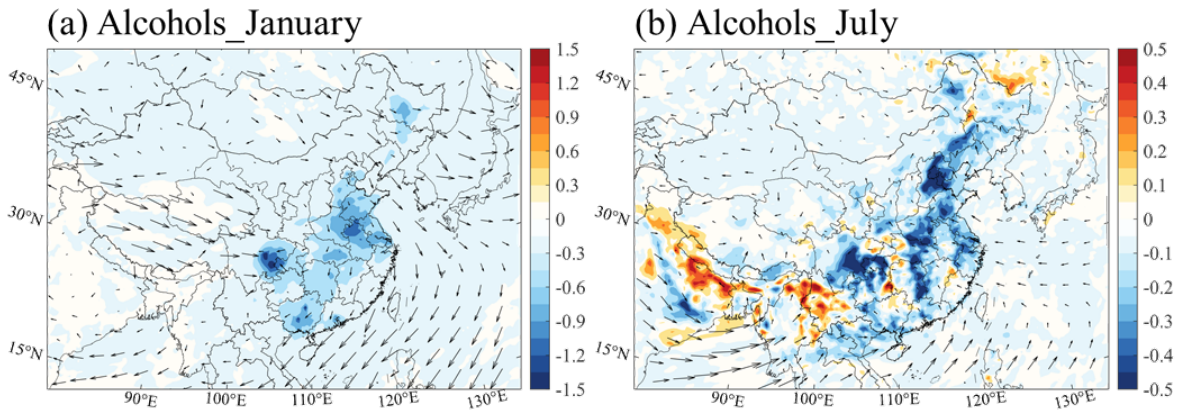

Figure S13. Changes in the monthly-averaged concentration of alcohols [Unit: pptv] response to the reduction in emission of *AVOCs* relative to *BASE* case in January (a) and July (b) of 2018. Arrows represent the wind speed and wind direction.

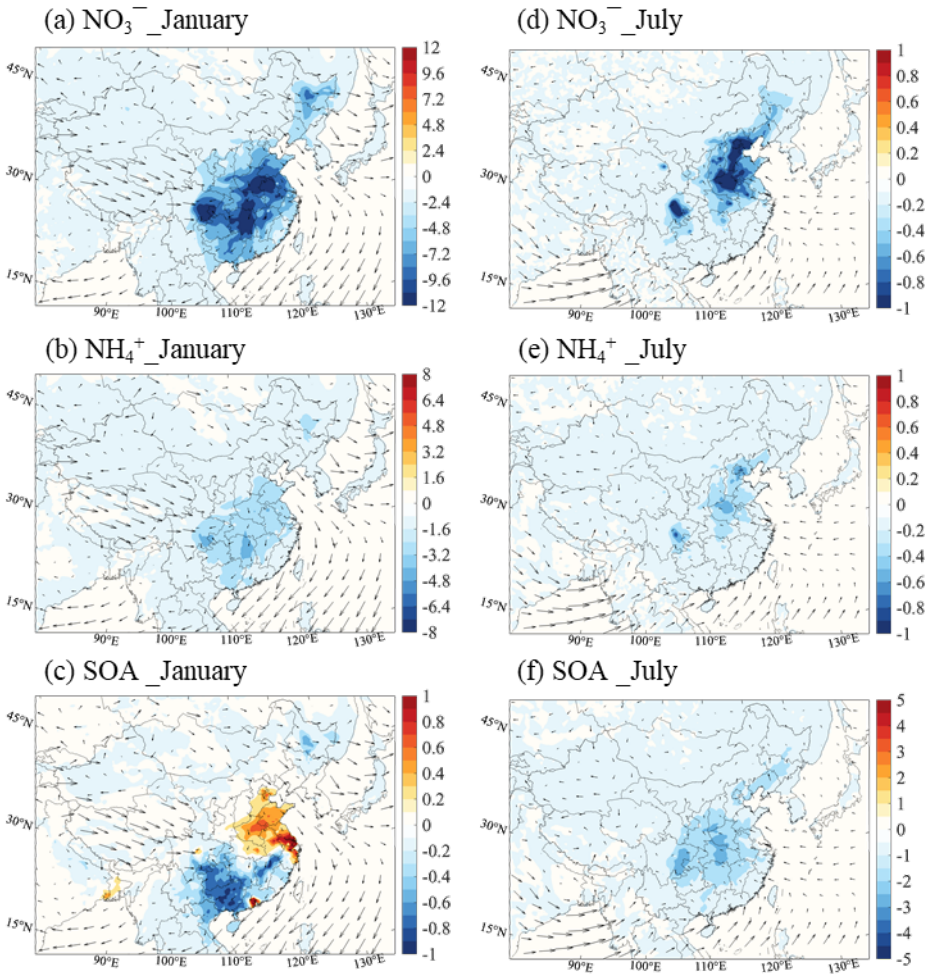

Figure S14. Changes in the monthly-averaged concentration of particulate nitrate (a, d) [NO_3^-; Unit: μg m^{-3}], particulate ammonia (b, e) [NH_4^+; Unit: μg m^{-3}], and Secondary Organic Aerosols (c, f) [SOA; Unit: μg m^{-3}] response to the ratio of 0.5 in NO_x emissions (*NO_x* case) in January (a-c) and July (d-f) of 2018. Arrows represent the wind speed and wind direction scaled by a factor of 5.

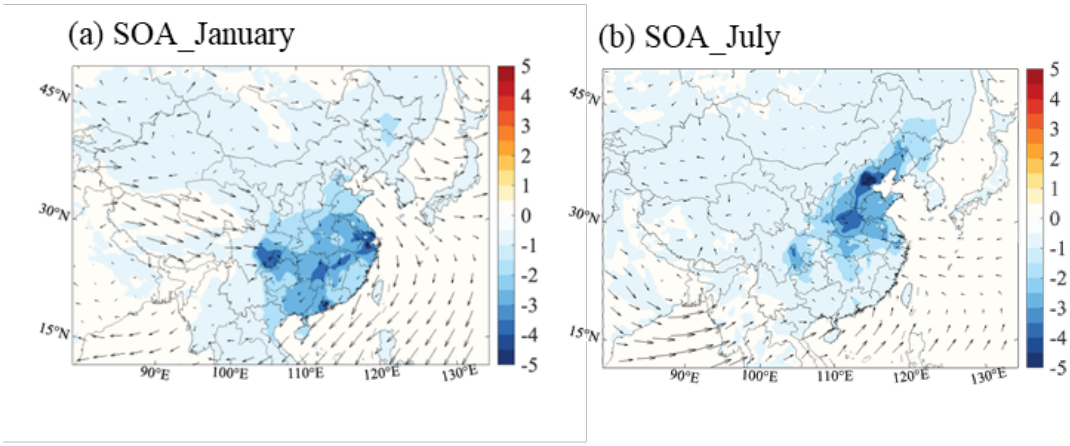

Figure S15. Changes in the monthly-averaged concentration of Secondary Organic Aerosols [SOA; Unit: μg m^{-3}] response to the ratio of 0.5 in AVOCs emissions (a, b; AVOCs case) in January (a) and July (b) of 2018. Arrows represent the wind speed and wind direction scaled by a factor of 5.

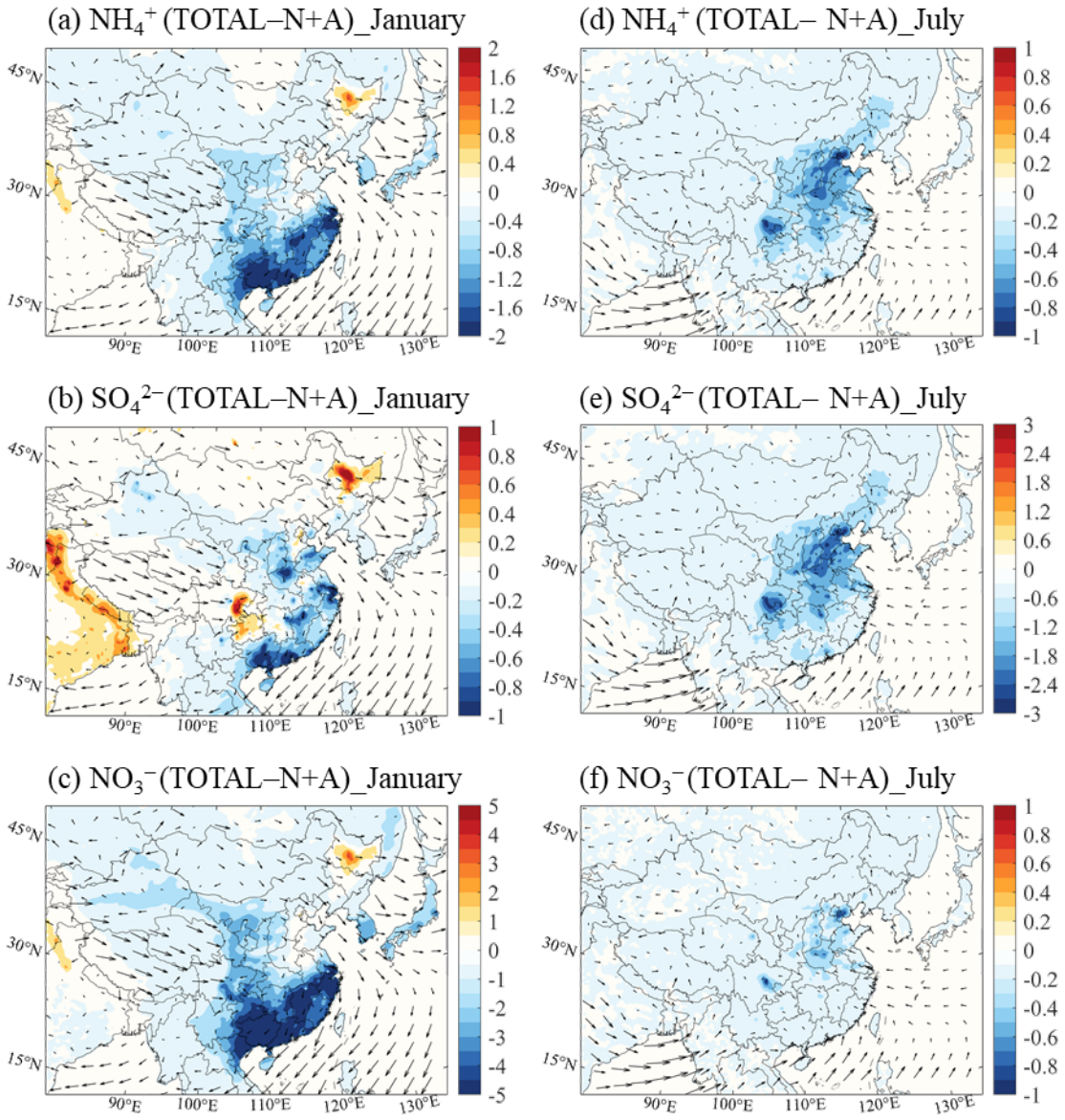

Figure S16. Changes in monthly-averaged concentration of particulate ammonia (a, d) [NH_4^+; Unit: μg m^{-3}], particulate sulfate (b, e) [SO_4^{2-}; Unit: μg m^{-3}], and particulate nitrate (c, f) [NO_3^-; Unit: μg m^{-3}] response to the *TOTAL* emissions case relative to *N+A* case in January (a-c) and July (d-f) of 2018. Arrows represent the scaled wind speed and wind direction.

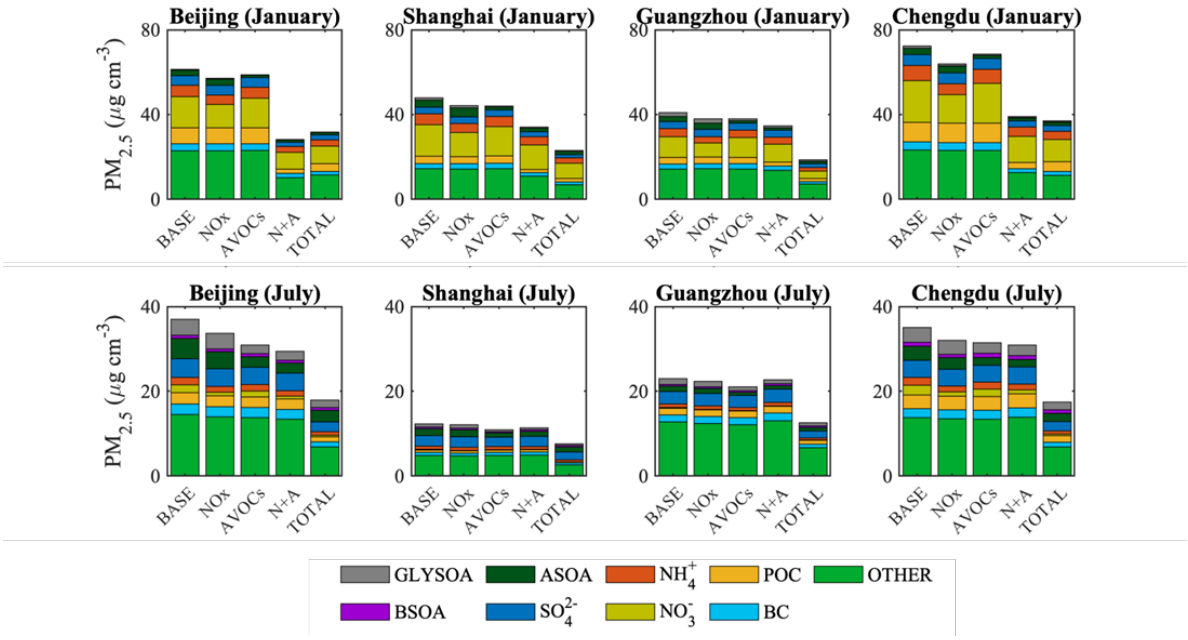

Figure S17. Averaged concentration of fine aerosols contributed by different species at four city sites (Beijing, Shanghai, Guangzhou, and Chengdu) in five simulated cases (*BASE*, *NOx*, *AVOCs*, *N+A*, and *TOTAL* cases) in January and July.

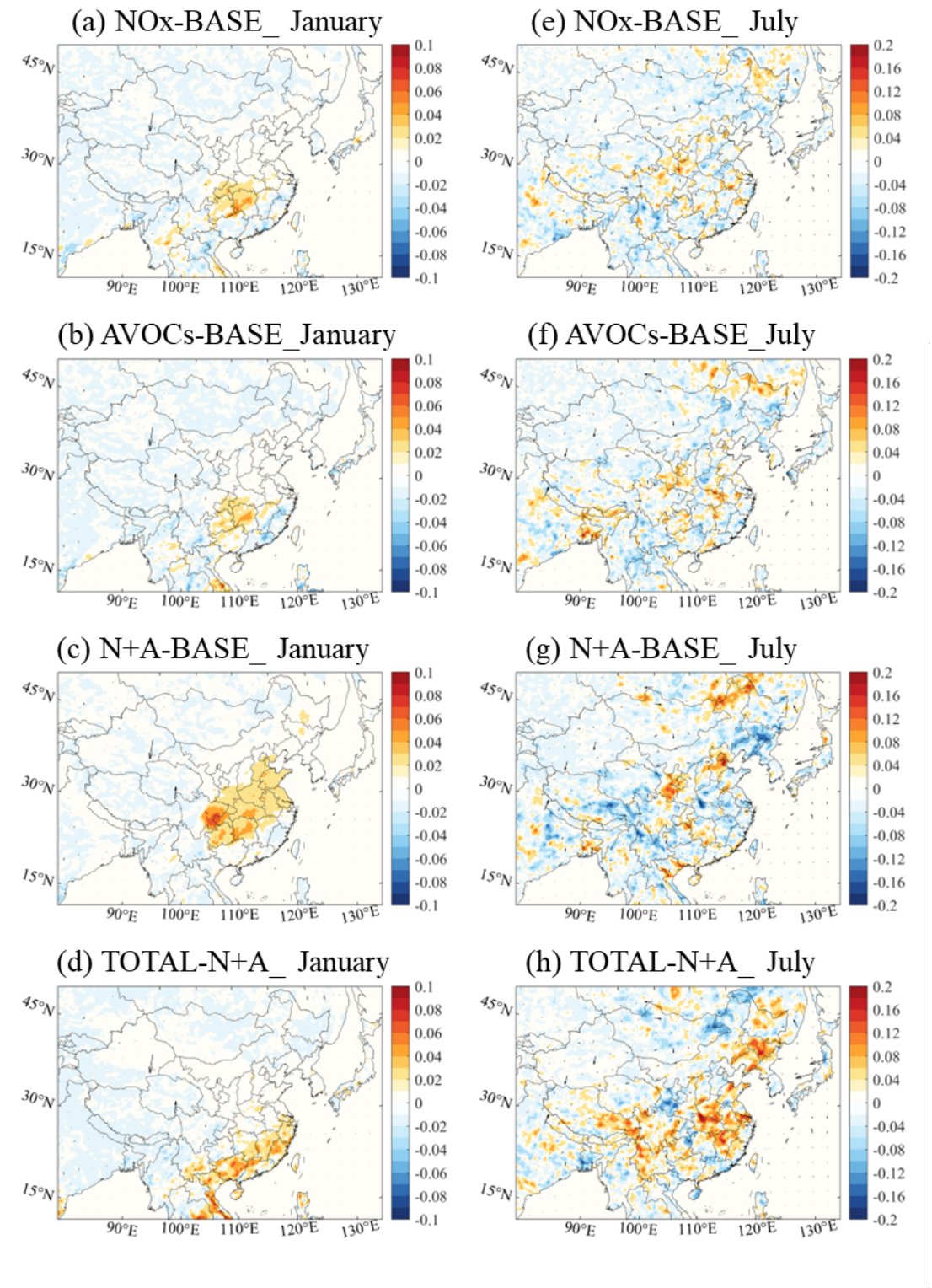

Figure S18. Changes in the monthly-averaged value of total photolysis rate (a-d) [Unit: s^{-1}] due to the emission reduction in NO_x (*NOx*; a,e), AVOCs (*AVOCs*; b,f), NOx and AVOCs (*N+A*; c, g) relative to the *BASE* case and *TOTAL* case relative to *N+A* cases(d, h) in January (a-d) and July (e-h) of 2018.

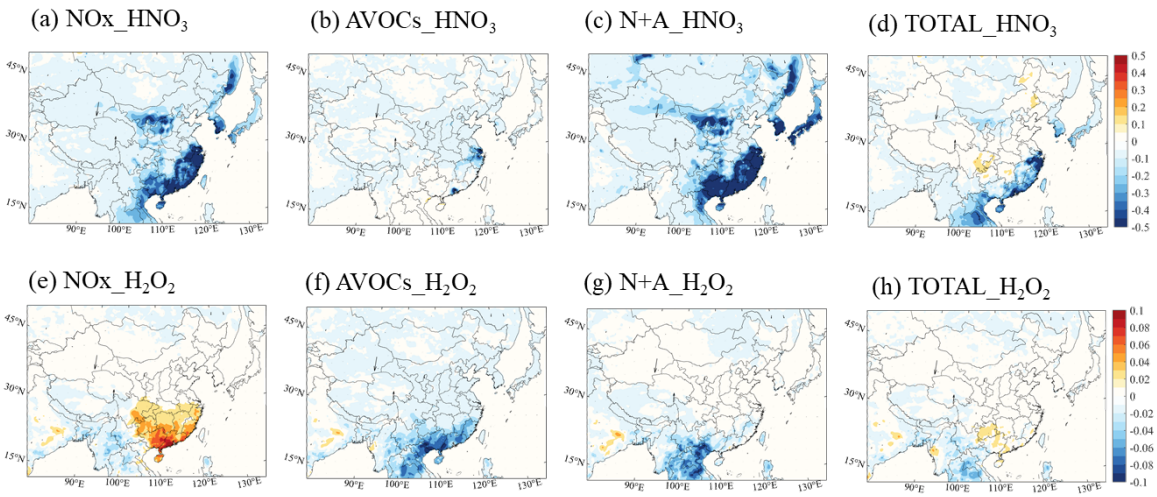

Figure S19. Changes in the monthly-averaged concentration of nitric acid (HNO_3) (a-d) and hydrogen peroxide (H_2O_2) (e-h) response to the *NOx* (a, e), *AVOCs* (b, f), *N+A* (c, g), and *TOTAL* (d, h) cases relative to *BASE* case in January of 2018.

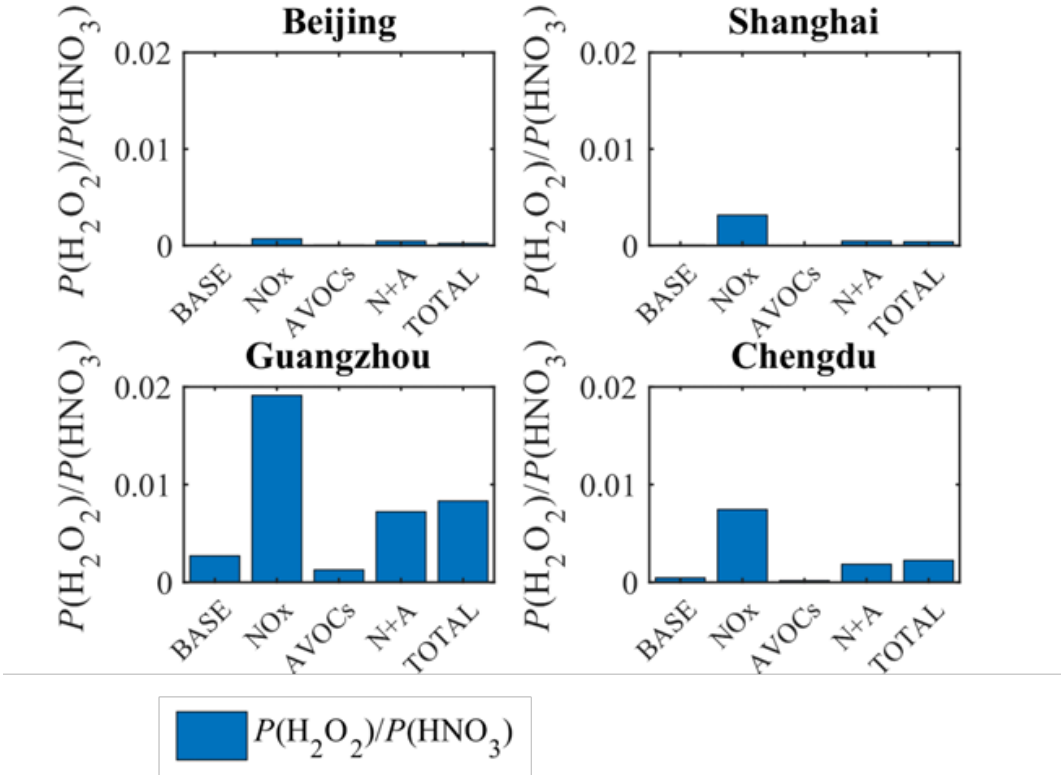

Figure S20. The averaged daytime value of ratio between the production rate of hydrogen peroxide (H_2O_2) and nitric acid (HNO_3) [$P(H_2O_2)/P(HNO_3)$] at four city sites (Beijing, Shanghai, Chengdu, Guangzhou) of China for January 2018 in the five emissions cases. The values of $P(H_2O_2)/P(HNO_3)$ shown in the figures are lower than 0.06, indicating the ozone sensitivity of VOC-limited at the four sites in five cases.

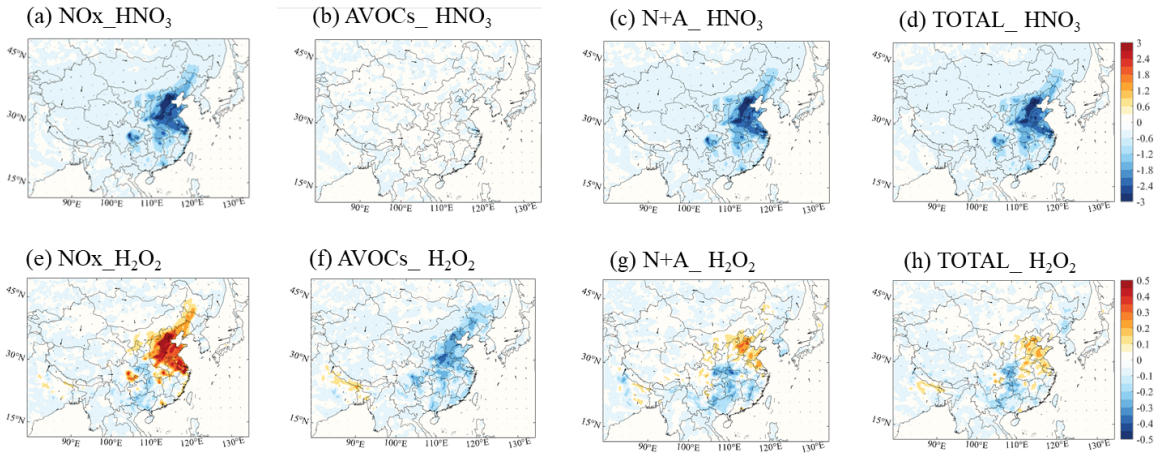

Figure S21. Changes in the monthly-averaged daytime concentration of nitric acid (HNO_3) (a-d) and hydrogen peroxide (H_2O_2) (e-h) response to the *NOx* (a, e), *AVOCs* (b, f), *N+A* (c, g), and *TOTAL* (d, h) cases relative to BASE case in July of 2018.

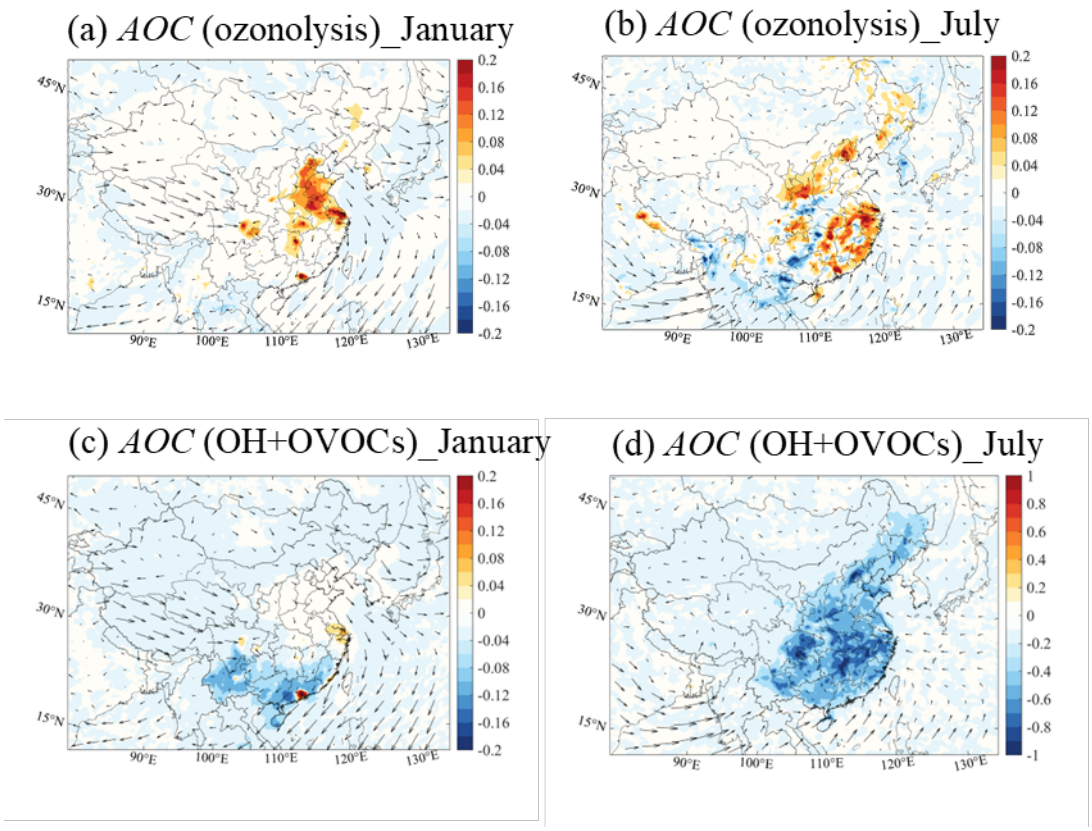

Figure S22. Changes in the monthly-averaged value of atmospheric oxidizing capacity (*AOC*) due to the reaction between alkenes and ozone (a, b; Unit: 10^6 molec. cm^{-3} s^{-1}) during nighttime (20:00 to 05:00 LST) and due to the reaction between OVOCs and OH radical in daytime (c, d; Unit: 10^7 molec. cm^{-3} s^{-1}) response to the NO_x emissions case relative to *BASE* case in January (a, c) and July (b, d) of 2018.

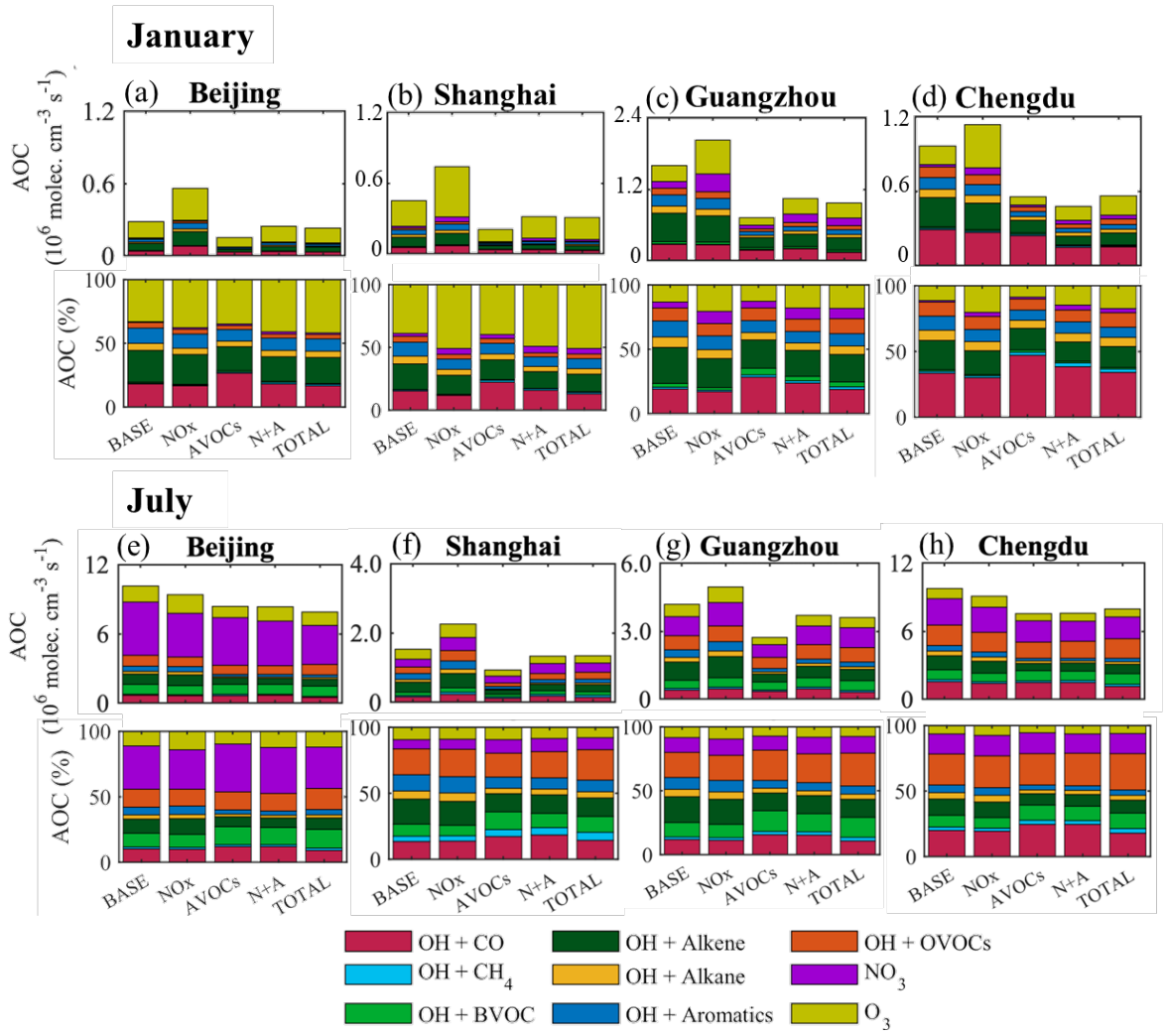

Figure S23. Averaged value and relative terms of nighttime *AOC* at the sites of Beijing (a, e), Shanghai (b, f), Guangzhou (c, g), and Chengdu (d, h) in five different simulated cases (*BASE*, *NOx*, *AVOCs*, *N+A*, *TOTAL* cases) in January (a-d) and July (e-h) of 2018. Notice the inconsistency in the scales.

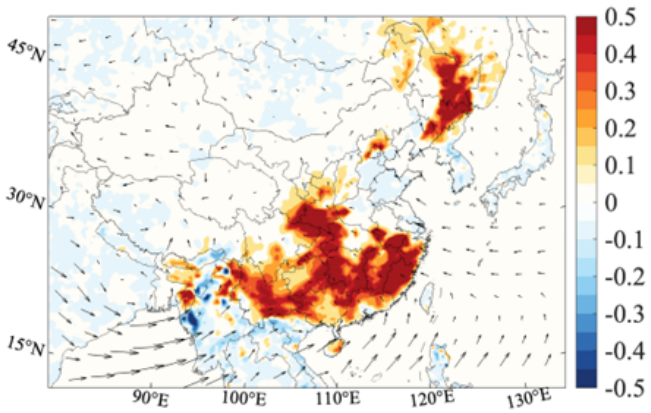

Figure S24. Changes in the monthly-averaged concentration of isoprene [Unit: ppbv] response to the reduction in the combined NO_x and AVOCs emissions case (*N+A* case) relative to the *BASE* case in July of 2018.

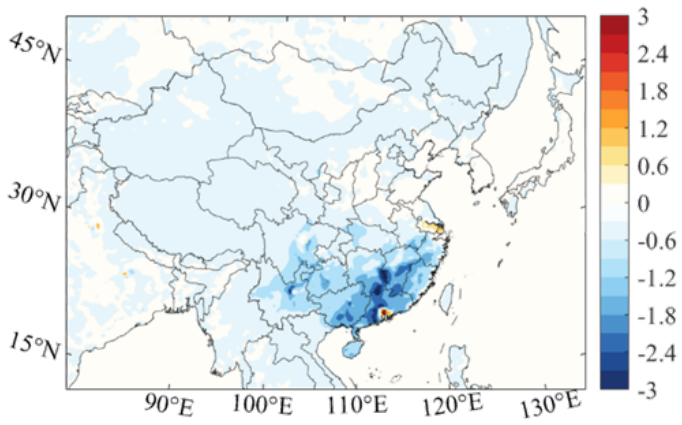

Figure S25. Changes in monthly-averaged value of daytime net production rate of odd oxygen [Unit: ppbv h^{-1}] response to the *NOx* emissions case relative to *BASE* case in January of 2018 (Net $P(O_x) = P(O_x) - D(O_x)$).